Inverse Estimation of the Mars Science Laboratory Entry Aerothermal Environment and Thermal Protection System Response

Milad Mahzari[*] and Robert D. Braun[†]

Georgia Institute of Technology, Atlanta, GA, 30332

Todd R. White[‡]

ERC Inc., Moffett Field, CA 94035

Deepak Bose[§]

NASA Ames Research Center, Moffett Field, CA 94035

The Mars Science Laboratory entry vehicle successfully landed the Curiosity rover on the Martian surface on August 5, 2012. A phenolic impregnated carbon ablator heatshield was used to protect the spacecraft against the severe aeroheating environments of atmospheric entry. This heatshield was instrumented with a comprehensive set of pressure and temperature sensors. The objective of this paper is to perform an inverse estimation of the entry vehicle's surface heating and heatshield material properties. The surface heating is estimated using the flight temperature data from the shallowest thermocouple. The sensitivity of the estimated surface heating profile to estimation tuning parameters, measurement errors, recession uncertainty and material property uncertainty is investigated. A Monte Carlo analysis is conducted to quantify the uncertainty bounds associated with the nominal estimated surface heating. Additionally, a thermocouple driver approach is employed to estimate heatshield material properties using the flight data from the deeper thermocouples while applying the shallowest thermocouple temperature as the surface boundary condition.

Nomenclature

B'	Dimensionless surface blowing rate
C_H	Heat transfer coefficient $= \rho_e u_e C_h$
C_h	Stanton number for heat transfer
C_p	Specific heat
h	Enthalpy
H_r	Total recovery enthalpy
$\dot{m}$	Surface blowing rate
q	Heat rate
t	Time
T	Temperature
α	Surface absorptivity
ϵ	Surface emissivity

---

[*]Graduate Research Assistant, Guggenheim School of Aerospace Engineering, AIAA Student Member.

[†]David and Andrew Lewis Professor of Space Technology, Daniel Guggenheim School of Aerospace Engineering, AIAA Fellow.

[‡]Research Scientist, Aerothermodynamics Branch, AIAA Member.

[§]Senior Research Scientist, Aerothermodynamics Branch, AIAA Associate Fellow.

American Institute of Aeronautics and Astronautics

κ	Thermal conductivity
ρ	Density
σ	Stefan-Boltzmann constant, standard deviation

Subscript and superscripts

c	Char
$cond$	Conduction
e	Boundary layer edge
g	Pyrolysis gas
rad	Radiative
s	Surface
v	Virgin
w	Wall
∞	Freestream

I.   Introduction

ABLATIVE materials are commonly used to protect atmospheric entry vehicles from the severe aerothermal environment they experience during the entry's hypersonic regime. There are significant uncertainties associated with the computational models used to predict an entry vehicle's surface heating in the Martian atmosphere and ablative materials thermal response.[1] These uncertainties have a significant effect on the Thermal Protection System (TPS) material selection and total mass, and therefore limit our ability to design more capable and robust Entry, Descent and Landing (EDL) systems. Flight data help with the quantification and possible reduction of design uncertainties. Mars Viking landers and Mars Pathfinder were the only Mars missions that were equipped with instruments that returned heatshield data during their atmospheric entries. A few studies have been performed to analyze the data returned by these missions; however, due to the limited nature of these datasets it is difficult to make any general conclusions about Mars entry aerothermal modeling based on the data from these missions.[2–6]

The Mars Science Laboratory successfully landed the Curiosity rover on the Martian surface on August 5, 2012. The MSL aeroshell was a 4.5-meter diameter spherically-blunted 70-degree half-angle cone with a triconic afterbody.[7] MSL's forebody heatshield was made of an ablative material called Phenolic Impregnated Carbon Ablators (PICA).[8] During the design phase, major uncertainties existed in the MSL's aerothermal environment due to the prediction of Boundary Layer Transition (BLT) early-on in the trajectory.[9] This resulted in the application of conservative assumptions for the design aerothermal environments including fully turbulent flow, supercatalytic wall and roughness heating augmentation. Based on these analyses and mission mass allocations, a uniform PICA thickness of 1.25 inch was used.[10, 11] In order to improve the state-of-the-art aerothermal modeling tools, the MSL heatshield was instrumented with a comprehensive set of pressure and temperature sensors called MSL Entry, Descent and Landing Instrumentation (MEDLI).[12] The aeroheating subsystem, called MEDLI Integrated Sensor Plug (MISP), provided subsurface temperature measurements of MSL's PICA heatshield at different locations and depths. The MEDLI dataset provided the first non-Earth entry aeroheating data since the Pathfinder mission, and more EDL data than all of the previous Mars missions combined.

In previous studies, the authors performed a preliminary post-flight analysis of the MSL's aerothermal environment and TPS performance.[13–15] Those studies included the presentation of the flight data, direct comparison of temperature data and thermal response model predictions, preliminary inverse estimation of surface heating and discussion of observed BLT from flight data. The current work advances the previous study by providing updated surface heating and material property estimations in addition to performing uncertainty and sensitivity analyses. Section II describes the MISP instrumentation and flight data. Section III presents the estimated surface heating profiles and provides sensitivity and Monte Carlo analyses to quantify the uncertainty associated with the estimated heating. Section IV discusses material property estimation using a thermocouple (TC) driver approach. This paper will focus on the inverse analysis of the flight data. References 16–18 discuss the forward comparison approach and ground testing efforts related to MISP instrument and PICA material properties.

American Institute of Aeronautics and Astronautics

II.   MISP Instrumentation

MEDLI consists of seven pressure ports and seven PICA plugs at different locations on the MSL heat-shield. The suite consists of three subsystems: MISP temperature/isotherm sensors, Mars Entry Atmospheric Data System (MEADS) pressure sensors, and Sensor Support Electronics (SSE). MISP sensors are installed into PICA plugs that are flush-mounted to the flight heatshield. The MISP plugs (Fig. 1a, T labels) are strategically placed to cover a broad range of heat rate environments, while the MEADS locations (Fig. 1a, P labels) are concentrated in the higher pressure and lower heat rate region near the stagnation point and the nose region.
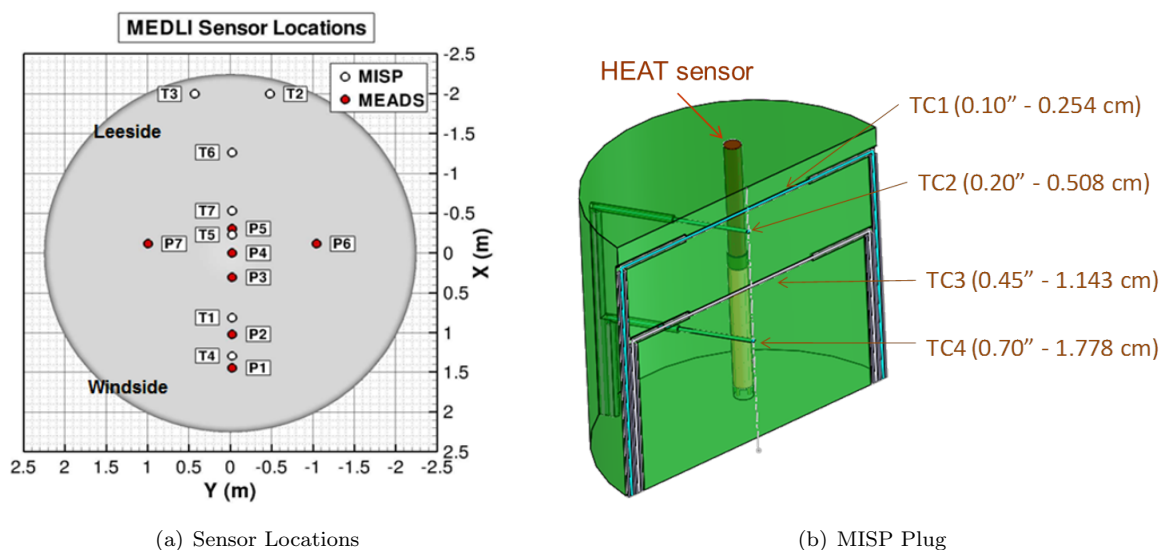

(a) Sensor Locations   (b) MISP Plug

Figure 1. Location of MEDLI sensors on MSL heatshield and schematic of MISP plug.[19]

Each MISP plug is 33 mm in diameter with a total depth of 29 mm, and contains four type-K U-shaped thermocouples. A schematic of a MISP plug is shown in Fig. 1b. The thermocouples are at nominal design depths of 2.54, 5.08, 11.43, and 17.78 mm (0.10, 0.20, 0.45, 0.70 inch) from the surface of the plug (see reference 13 for X-ray measured actual depths of each thermocouple). The top two thermocouples were intended primarily for aerothermodynamic reconstruction and are sampled at 8 Hz, while the two deeper thermocouples were primarily intended for material property reconstruction and are sampled at 1 or 2 Hz depending on the location. Data from TC3 and TC4 thermocouples in plugs 5 and 7 are not recorded because of data channel limitations. Each MISP plug also contains an isotherm sensor called Hollow aErothermal Ablation and Temperature (HEAT).[20, 21] HEAT is an improved version of a similar sensor that was used for the Galileo entry probe to determine surface recession.[22] However, at the lower heat rates experienced during Martian entry, it is not expected to provide any information on recession. The sensor elements are conductive, so as the char layer-virgin material interface advances, these elements become shorter and the voltage output decreases. The HEAT sensor voltage measurements can be correlated with the sensor length which can then be correlated with char depth. The HEAT sensor is sampled at 8 Hz.

The MEDLI data were recorded and stored successfully during the atmospheric entry. A limited part of the data was transmitted in real-time and the full dataset was received from the rover within a week after landing. The thermocouples behaved as expected and the data contained a low amount of noise. The HEAT sensor however did not behave as expected and the recorded transient data were very noisy. For this reason, the analysis of HEAT data is not pursued in this work. The flight data are not shown in this paper for the sake of brevity and the readers are suggested to consult references 13, 14 and 15 for the presentation of the flight data and discussions of direct observations from the thermocouple temperature profiles. The current study will focus on the inverse analysis of the data. In this paper, time zero is assumed to be the entry interface time corresponding to a spacecraft time (SCLK) of 397501714.953125 seconds.

American Institute of Aeronautics and Astronautics

III.   Surface Heating Estimation

Aerothermal heating and ablative material response are naturally coupled physical phenomena; however, they are often treated in an uncoupled fashion for design. Computational Fluid Dynamics (CFD) tools are used to predict the aerothermal heating of an entry vehicle based on time-varying trajectory information such as velocity, atmospheric density, angle of attack and sideslip angle. Langley Aerothermodynamic Upwind Relaxation Algorithm (LAURA)[23] and Data Parallel Line Relaxation (DPLR)[24] are the state-of-the-art NASA codes that were used for the calculation of MSL surface heating. These CFD tools predict the aerothermal environment by typically assuming a radiative equilibrium wall and certain wall catalicity and turbulence models. TPS material response including ablation, pyrolysis and heat conduction into the material are often neglected at this analysis stage. Surface boundary conditions are derived from CFD solutions and are then used as inputs to heatshield ablation and thermal response tools. Fully Implicit Ablation and Thermal response (FIAT)[25] program is the standard NASA code used today for ablative material thermal response modeling. FIAT simulates 1-D heat conduction, material decomposition and pyrolysis gas generation and surface ablation using equilibrium chemistry models. In this study, FIAT will be used to simulate heatshield material in-depth temperature response and syrface energy balance.

MISP data include in-depth temperature measurements of the heatshield; therefore, the surface heating cannot be derived directly from the flight data, meaning that the reconstruction of surface heating must be posed as an inverse problem. Inverse heat transfer problems often involve the estimation of a boundary condition such as surface heating or temperature, or the estimation of model parameters such as material thermophysical properties.[26-28] Estimation of time-dependent surface heating belongs to the class of function estimation problems, as they require the identification of many points in time. Inverse methods attempt to estimate the surface heating by minimizing an objective function of the difference between analytical model predictions (FIAT temperature calculations) and measurements (MISP temperature data). A commonly used function for this difference calculation is the sum of squared differences (ordinary least squares).

Two classes of methods are typically used for surface heating estimation: whole-time domain methods and sequential methods. Whole-time domain methods iteratively estimate the entire heating profile using the entire measurement range, while sequential methods estimate the surface heating at a given time using a limited subset of the measurements and proceed sequentially in time. Sequential methods can be more efficient if set up properly; however, whole-time domain methods are typically more stable and can be more easily integrated with FIAT. Therefore in this study, an iterative whole-time domain method called the Gauss-Newton method will be used. It is a modification of Newton's minimization method applicable to nonlinear least squares problems which does not require the knowledge of second derivatives; however, it requires the time-consuming computation of the first-derivative Jacobian matrix. This finite difference computation requires hundreds of FIAT simulations at each iteration.

Inverse problems are mathematically ill-posed, meaning that conditions of solution existence, uniqueness and stability are not guaranteed. These problems can be unstable in the presence of data/model errors or when large numbers of parameters are estimated. This can result in significant oscillations that lead to inaccurate or non-physical estimation results. Regularization techniques can be used in conjunction with the Gauss-Newton minimization scheme to make the problem better posed and more stable. Regularization has a smoothing effect on the parameter estimates. Andrey Tikhonov devised a procedure for the regularization of ill-posed problems.[29] His technique involves the addition of a penalty function to the ordinary least-squares objective function to alleviate oscillations in the solution. This penalty term is composed of a squared difference function of the surface heating profile estimation points and can take various forms (0th,1st and 2nd order). For example, the zero-order function is equal to the sum of squares of estimation points while the first-order function is equal to the sum of squared differences of consecutive estimation points. The level of regularization can also be adjusted using a scaling parameter.[28] A more detailed description of the Gauss-Newton algorithm and Tikhonov regularization method can be found in reference 13.

In this analysis we will use the shallowest thermocouple data (TC1) for the purpose of surface heating estimation as it is the most sensitive to surface heating and least affected by subsurface material property uncertainty. Heating estimation is performed every 1 second (1 Hz) using flight data at a frequency of 2 Hz. Two distinct approaches are used. The first approach reconstructs the surface heating by estimating heat transfer coefficient at an ablating surface with surface recession. Due to the limitations of this approach for MSL heating conditions, a second approach is also employed which directly estimates surface heating at a non-receding surface.

American Institute of Aeronautics and Astronautics

A. Heat Transfer Coefficient Estimation of an Ablating Surface

For an ablative material, surface heat rate is not a direct input to FIAT. Surface heating is modeled with a surface energy balance equation which represents many physical phenomena that occur at the surface of an ablative material. This equation (called "option 1" in FIAT) is:

$$C_H(H_r - h_w) + \dot{m}_g h_g + \dot{m}_c h_c - (\dot{m}_c + \dot{m}_g) h_w + \alpha_w q_{rad} - \sigma \epsilon_w (T_w^4 - T_\infty^4) - q_{cond} = 0 \qquad (1)$$

The first term represents the sensible convective heat rate. The sum of the second, third and fourth terms defines the total chemical energy at the surface due to the ablation products and pyrolysis gas. The fifth and sixth terms are the incoming radiative heat rate absorbed by the material and the reradiation to the environment. The last term in Eq. (1) represents the rate of heat conduction into the TPS material. As mentioned before, surface heating is calculated by CFD tools assuming radiative equilibrium wall and certain catalytic and turbulence models. Based on CFD solutions, the total recovery enthalpy, H_r, and wall enthalpy, h_w, can be determined. Knowing these values and the CFD-predicted convective heat flux, the surface heat transfer coefficient, C_H, is calculated. C_H, H_r, surface pressure, and the blowing reduction parameter are input to FIAT as functions of time. It should be noted that the CFD heat transfer coefficient values are unblown, and FIAT corrects the input C_H for heating reduction due to pyrolysis gas blowing.[25] Pre-calculated equilibrium wall chemistry solutions (B' tables) are input to FIAT for a given material and the surface energy balance is solved iteratively using the boundary condition inputs from CFD and the B' tables. In doing so, FIAT calculates its own wall enthalpy and temperature which are often not equal to the CFD-calculated values due to the usage of different surface energy balance approaches.

Many of the parameters in Eq. (1) can affect the subsurface thermocouple temperature and the surface heating estimate. Some of these parameters are inputs to FIAT while others are calculated internally by FIAT. While it is desirable to have an accurate knowledge of all these terms, they are not all directly observable from the flight data and any attempt to simultaneously estimate multiple parameters leads to non-unique solutions. The authors have traditionally defined the inverse problem as the estimation of the time-dependent heat transfer coefficient profile. This approach was used for the inverse analysis of simulated MISP data[30] and Mars Pathfinder data.[6] Inverse methods are used to estimate heat transfer coefficient as a function of time while keeping recovery enthalpy fixed to the CFD-calculated value and allowing FIAT to internally calculate surface ablation chemistry and material decomposition. This approach was naturally used in the preliminary inverse estimation of MSL surface heating.[13]
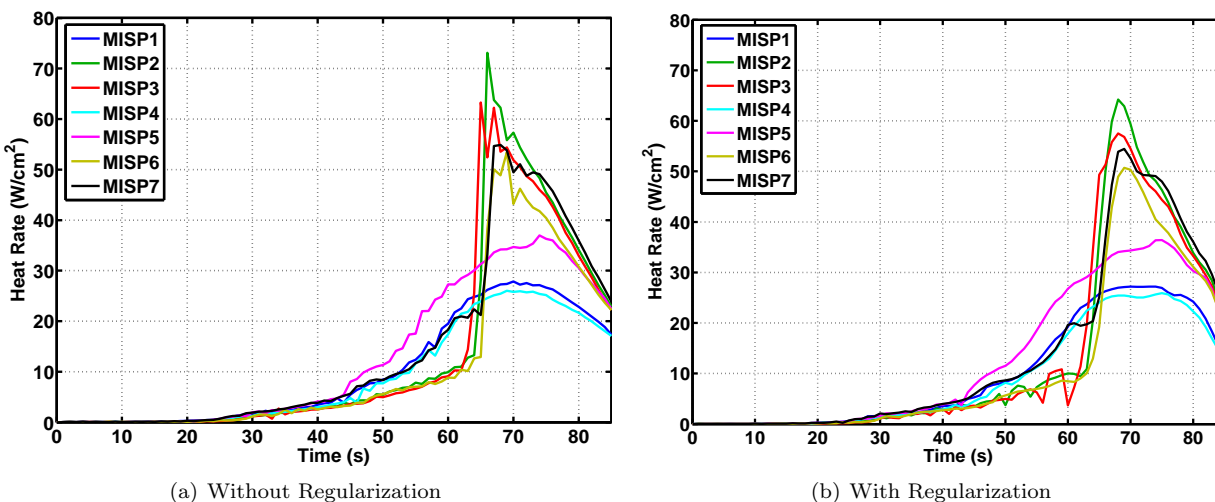

(a) Without Regularization

(b) With Regularization

Figure 2. Reconstructed surface heat rate profiles at MISP locations using the C_H estimation approach.

Figure 2 shows the estimated surface heating profiles at all MISP locations using the heat transfer coefficient approach. The heat rate in this figure is the summation of the convective and chemical energy at the surface (the sum of the first four terms in Eq. (1)). Both unregularized and regularized solutions are shown. While unregularized solution results in a better match with the in-depth temperature data, we can clearly see that regularization reduces the oscillations and provides a more physically realistic heat rate

American Institute of Aeronautics and Astronautics

profile. Comparison of the heat rate profiles for different plugs leads to the observation that MISP5 has the highest heating up to about 65 seconds followed by plugs 1, 4 and 7, while the plugs close to the shoulder (2, 3, and 6) remain at a low level of heating. This trend matches the laminar heating predictions by CFD tools at the apex region (plugs 5 and 7) and stagnation region (plug 1 and 4) which were expected to experience the highest laminar heating. However, we can clearly observe the onset of BLT around the 63-65 second period for plugs 3, 2, 6 and 7. BLT results in much higher turbulent heating levels for these plugs. Plugs 2, 3 and 6 match the trends predicted by CFD tools; however, plug 7 significantly exceeds CFD predictions. This can be attributed to heating augmentation due to surface roughness or shock-layer radiation. Additional analysis will be required to investigate this observation. The small spike in plug 5's surface heating around 74 seconds may also be BLT. Similar to plug 7, surface heating at plug 5 also exceeded the CFD predictions and can be attributed to the same reasons. Plugs 1 and 4 remained laminar throughout the trajectory, but slightly exceeded the CFD predictions. Preliminary analysis shows that the observed difference can be partially explained by radiative heating in the stagnation region, although more work is needed.[18]

Some limitations and uncertainties exist in the heat transfer coefficient approach for MSL heating conditions. This approach relies on equilibrium models for the calculation of surface chemistry terms. As long as the material ablation model is accurate, the heat transfer coefficient estimation is accurate too. However, the equilibrium chemistry model employed in FIAT for PICA is known to be inaccurate at the low heating conditions experienced by MSL ($< 100\ W/cm^2$) and it tends to overpredict the recession.[31] As a matter of fact, the model's recession prediction for the nominal MSL heating environment exceeds TC1 depth. This is clearly not accurate because flight data suggest that recession was less than 0.10 inch as all thermocouples survived.[13] Figure 3 compares the nominal CFD-calculated recovery enthalpy and FIAT-calculated wall enthalpy profiles at plugs 1 and 2. As mentioned before, this wall enthalpy is calculated by FIAT's PICA equilibrium model and does not match the CFD-calculated wall enthalpy. It can be clearly observed that the two enthalpy profiles approach one another around 80-85 seconds. This leads to convective heat rate (first term in Eq. (1)) approaching zero which results in the loss of in-depth temperature sensitivity to C_H. For this reason, in the heat transfer coefficient approach, estimation is ceased around 85 seconds as a close match between the FIAT temperature predictions and TC1 flight data can not be achieved through C_H adjustment after this time.
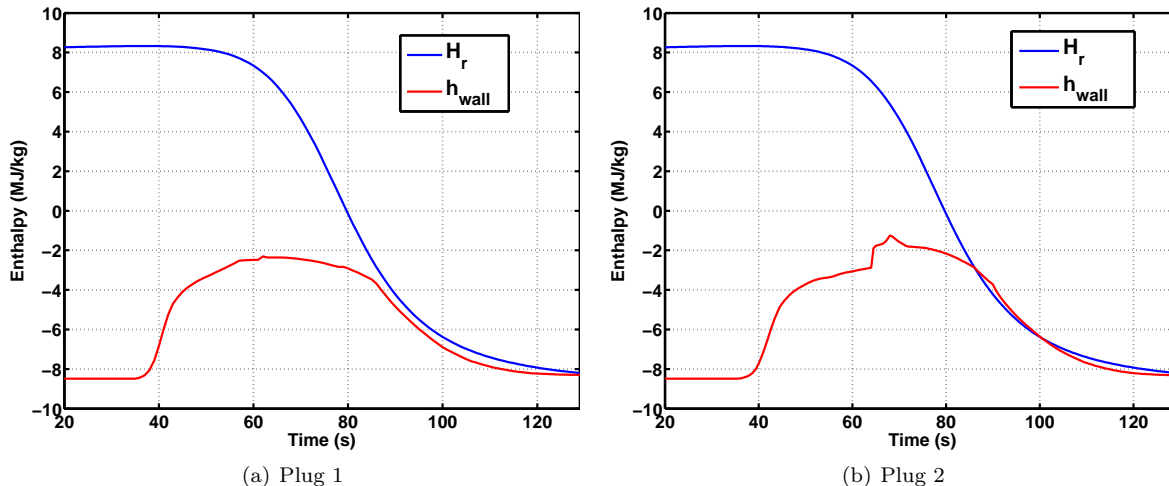

(a) Plug 1   (b) Plug 2

Figure 3. Recovery enthalpy and FIAT wall enthalpy compared at plugs 1 and 2.

B. Heat Rate Estimation of a Non-Receding Surface

No validated finite-rate models exist for PICA gas-surface chemistry in the Martian atmosphere. Consequently, the observed lack of substantial recession in flight and the known overprediction by FIAT equilibrium chemistry models motivate the application of another bounding approach where surface heating is estimated without recession. Recession can not simply be turned off in Eq. (1) without regenerating the chemistry solutions; therefore, C_H estimation is not possible for this approach. An alternative surface energy balance option is implemented in FIAT (called "option 3") which can be reformulated into the following equation:

American Institute of Aeronautics and Astronautics

$$q_s + \alpha_w q_{rad} - \sigma \epsilon_w (T_w^4 - T_\infty^4) - q_{cond} = 0 \qquad (2)$$

The first term in this equation is analogous to the sum of the first four terms in Eq. (1) (reported as the surface heat rate in the previous section) which includes the convective heat flux and chemical heating contributions. This approach allows us to suppress surface recession, thus estimating a non-receding surface heat rate using the inverse methods described earlier. Being independent of FIAT surface chemistry models, this approach enables a more accurate estimation of the surface heating profile for the entire time period. The estimation is not limited to 0-85 seconds as it was with the C_H approach. Figure 4 shows the unregularized and regularized surface heating estimates at all MISP plug locations. The estimation was performed as in the previous section by using the Gauss-Newton method in conjunction with Tikhonov regularization technique, and only TC1 data were used.

(a) Without Regularization
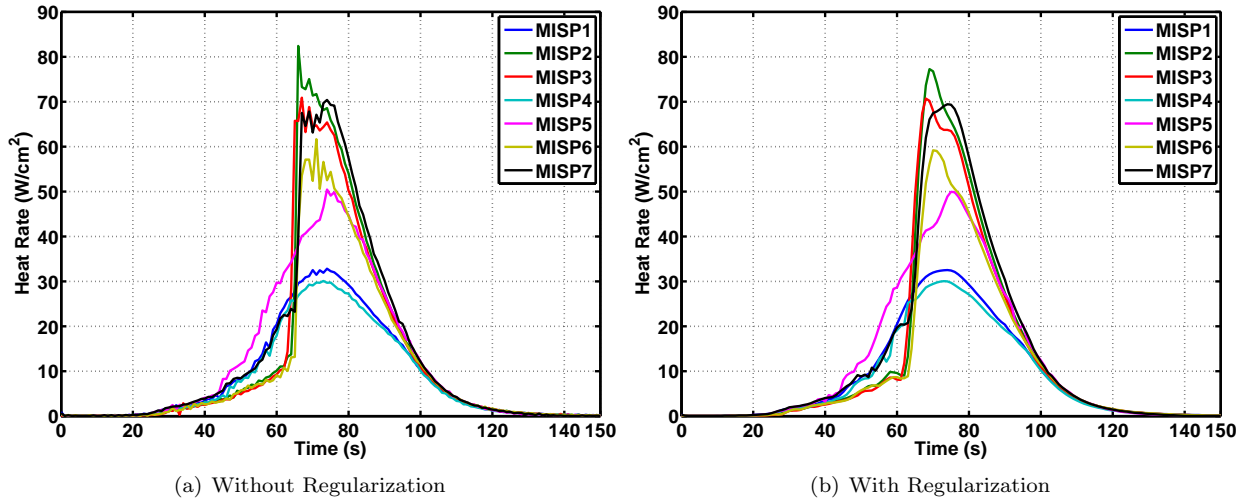
(b) With Regularization

Figure 4. Estimated non-receding surface heat rate profiles at MISP locations.

The same laminar and turbulent heating trends observed in the first approach (Fig. 2) can also be seen here. In general, the estimated surface heating is higher for this approach. In the absence of recession, the surface is farther away from TC1 and consequently higher incoming heating is required to achieve the same in-depth temperature. We can also see that the regularized solutions provide smoother and more physically realistic heating profiles than the unregularized solutions. Nonetheless, the unregularized solutions match the data more accurately. Some uncertainties are associated with these estimates due to numerical issues, measurement errors, recession uncertainty and material property variations. The next sections examine the effect of these uncertainties on the estimated non-receding surface heat rate profile mainly at plug 2 (highest heating case). Similar results are expected at other locations.

1. Numerical Sensitivity

Numerical sensitivity study allows us to show that the estimated heat rate profiles are stable and robust to numerical parameters. Four parameters are examined here: regularization order, regularization parameter, data frequency and heat rate estimation frequency. Figure 5 shows the effect of regularization order. As mentioned before, regularization has a smoothing effect on the estimated heating profile. Minor differences can only be observed in the peak region (67-74 seconds) in Fig. 5a. Lower order of regularization results in higher level of damping. In Fig. 5b, we can see that the match between the data and FIAT predictions is similar for all three cases. First-order regularization is typically used in literature for surface heating estimation problems and will be applied in this analysis.

The plots in Fig. 6 show the effect of the regularization parameter, which is a scaling factor that controls the level of smoothing. Estimation without regularization results in a very good match between FIAT TC1 temperature predictions and the flight TC1 data. The difference is within 1 K as shown in Fig. 6b. However, Fig. 6a shows that the reconstructed heat rate profile includes some oscillations around the peak heating time. As the regularization parameter is increased, the oscillations are reduced and the estimated heat
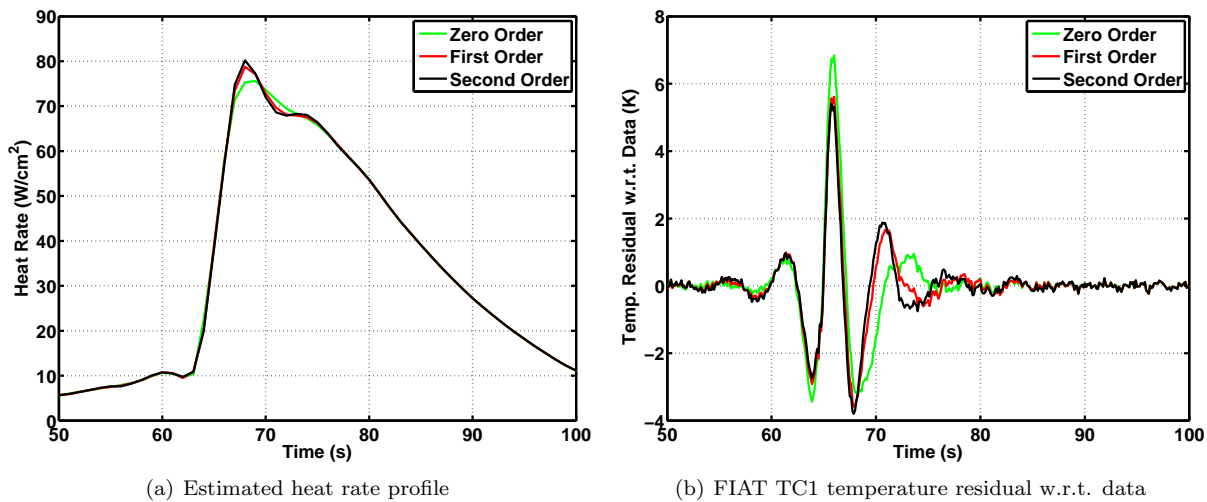
American Institute of Aeronautics and Astronautics

(a) Estimated heat rate profile

(b) FIAT TC1 temperature residual w.r.t. data

Figure 5. Effect of regularization order on surface heating estimation results at plug 2.

(a) Estimated heat rate profile

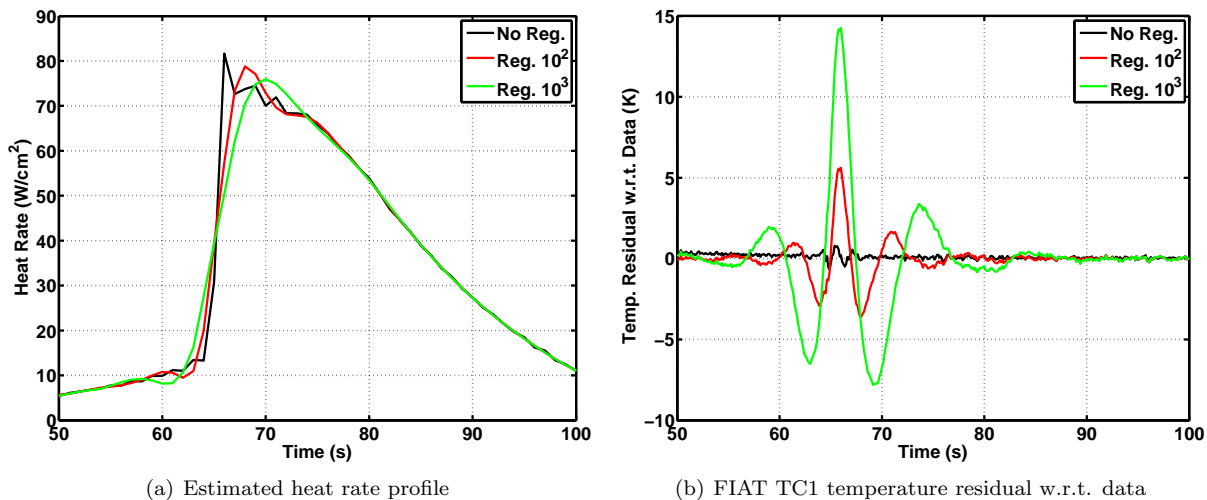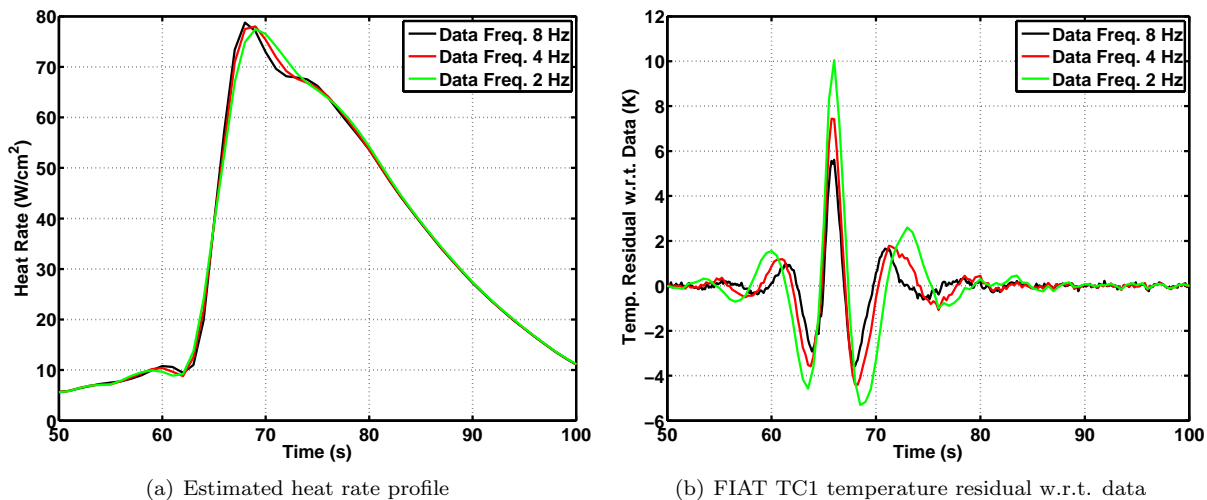(b) FIAT TC1 temperature residual w.r.t. data

Figure 6. Effect of regularization parameter on surface heating estimation results at plug 2.

rate profile takes a shape which is more similar to CFD-generated profiles. However, we can see that the regularization dissipates the sharp rise due to turbulent transition. We can also see in Fig. 6b that a higher parameter value results in a worse match between FIAT temperature predictions and TC data. Consequently, a baseline regularization parameter of 10^2 was selected in this work as a balance between smoothing and data matching.

For most plugs, the TC1 temperature data are available at 8 Hz. However, selection of the data frequency used in the inverse analysis should be approached carefully. Using the original 8 Hz data in the estimation would require significant computer time as FIAT simulations have to be performed and saved at a high rate. A lower data frequency is desirable because it lowers the computational cost in addition to providing an inherent smoothing of the data through interpolation. However, one needs to ensure that the estimation problem remains over-determined, meaning that there should be more measurement points than estimation parameters. For example, if the surface heating is estimated at 1 Hz, the data frequency should be higher than 1 Hz. Figure 7a illustrates the effect of data frequency on estimated surface heating profile. Data frequency does not have a significant effect on the surface heating estimation results. However, a mild smoothing effect is evident as the data frequency is reduced. This is related to the inherent smoothing of the data that occurs when the original data are interpolated at a lower frequency.
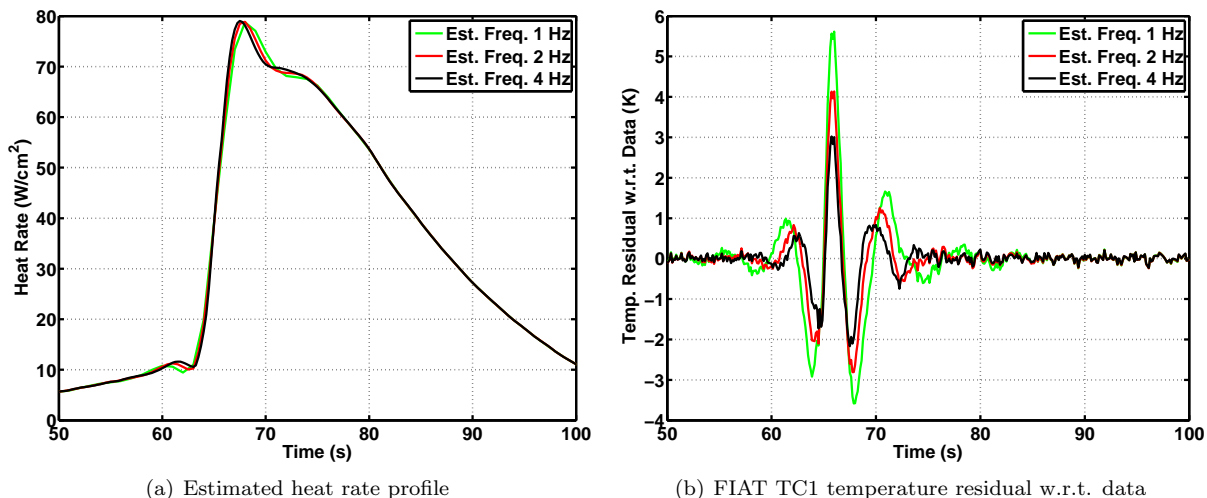
Figure 8 shows the effect of estimation frequency. Higher estimation frequency results in the reconstruction of surface heating at a higher time resolution; however, it requires more computational resources. We

American Institute of Aeronautics and Astronautics

(a) Estimated heat rate profile

(b) FIAT TC1 temperature residual w.r.t. data

Figure 7. Effect of data frequency on surface heating estimation results at plug 2.

(a) Estimated heat rate profile

(b) FIAT TC1 temperature residual w.r.t. data

Figure 8. Effect of estimation frequency on surface heating estimation results at plug 2.

can see that for higher estimation frequency, turbulent transition is captured only slightly more accurately than for the lower estimation frequency case. The temperature residual with respect to flight data is smaller; however, the overall effect is still minimal.

This numerical sensitivity analysis showed that the estimated heat rate profiles are robust with respect to numerical parameters. Therefore, for the rest of the analysis in this paper we will use the first order regularization with a parameter of 10^2, data frequency of 2 Hz and estimation frequency of 1 Hz. This will allow us to obtain numerically accurate smooth solutions while lowering the computational cost.

2. Measurement Error Sensitivity

Two types of measurement errors are examined here: TC depth uncertainty and thermal lag. Accurate flight heatshield TC depths using X-ray measurement are available; however, this measurement technique can have an uncertainty up to ± 0.003 inch. Figure 9a shows the effect of this uncertainty on the estimated heating profile at plug 2. The deviation resulting from this uncertainty is bounded by $\pm 4 \ W/cm^2$ at the peak.

Additionally, the TC temperature readings may contain a thermal lag bias error. Thermal lag is caused by the thermal mass of the thermocouple and is defined as the difference between the material temperature and the thermocouple reading. Figure 9b shows the surface heating profile estimated from temperature data corrected for a constant 1-second lag (partially based on ground testing of MISP instrumentation). We can see that the thermal lag correction results in a 1-second shift in the estimated heating profile.
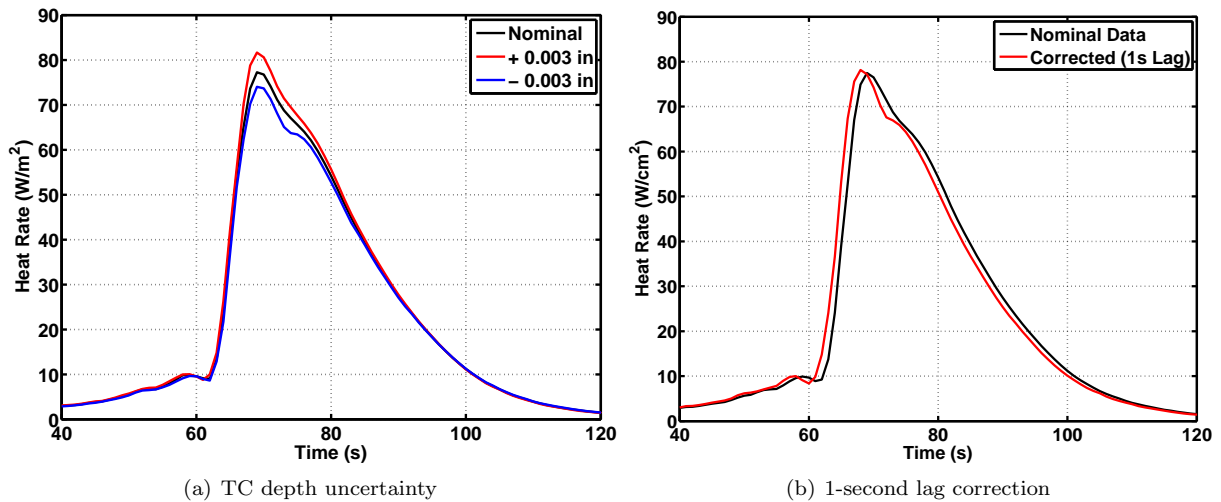
American Institute of Aeronautics and Astronautics

(a) TC depth uncertainty

(b) 1-second lag correction

Figure 9. Effect of measurement errors on surface heating estimation results at plug 2.

3. Recession Sensitivity

The heat rate estimation approach used in this section assumes zero surface recession because the nominal PICA ablation model significantly overpredicts recession for MSL conditions. The only information obtained from flight data regarding recession is that it was less than 0.10 inch (TC1 depth) as the shallowest thermocouples did not burn out. Therefore, it is desirable to examine the effect of surface recession on the estimated heating profile.

Once the non-receding surface heat rate profile is estimated, the complete in-depth material response is known. The temperature and heat conduction are known as functions of time at any depth between the original surface and the TC1 location. If we assume that the surface is at a specific depth at a given time, we can calculate the required surface heat rate which would maintain the same in-depth thermal response. In equation 2, all the parameters in the second, third and fourth terms are known at any location and time; therefore, the first term can be readily calculated for the entire time and depth domain, thus creating an estimated surface heat rate map for varying surface locations (Fig. 10a). The surface heat rate can then
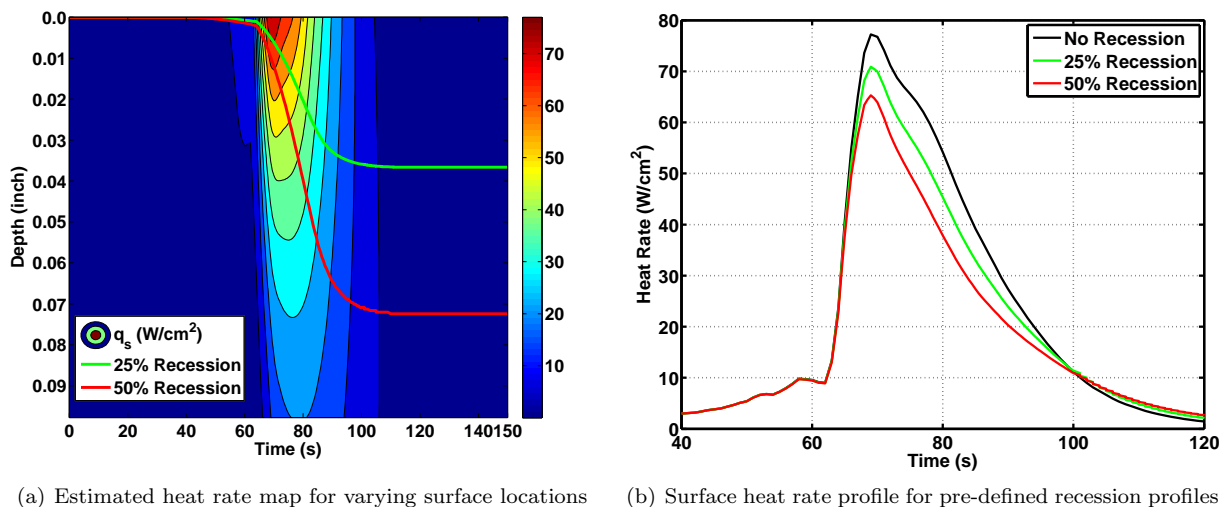

(a) Estimated heat rate map for varying surface locations

(b) Surface heat rate profile for pre-defined recession profiles

Figure 10. Effect of surface recession uncertainty on heating estimation results at plug 2.

be estimated for a pre-defined recession profile using this map. A reasonable approach for choosing such a recession profile is to scale the recession profile calculated by the nominal PICA ablation model for the nominal heating environments. Recession profiles scaled to 25% and 50% are overlayed on the surface heat

American Institute of Aeronautics and Astronautics

rate map shown in the same figure. Figure 10b shows the estimated surface heat rate for these pre-defined recession profiles. We can see that increased surface recession results in a lower estimated surface heating because the surface becomes closer to TC1, requiring a lower surface heating to maintain the same in-depth temperature response. It can also be observed that the recession sensitivity is not significant in the first 65 seconds when surface recession is small.

4. Material Property Sensitivity

Figure 11 shows the sensitivity of the estimated surface heating profile at plug 2 to perturbations in different PICA material properties. For this sensitivity analysis, a fixed ±10% perturbation is applied to both virgin and char properties. In Fig. 11a, we can see that an increase in material density results in higher estimated surface heating for the entire time period. Higher density means a higher material thermal mass and consequently a higher surface heating is required to maintain the same temperature response. The effect is most visible around the peak region. Pre-flight density measurement of the MISP plugs indicated only a ±1.5% variation in virgin density; therefore, the effect of density uncertainty on estimated surface heating is expected to be small. Figure 11b shows the effect of thermal conductivity perturbation. It can be observed

(a) Density perturbation

(b) Thermal conductivity perturbation

(c) Specific heat perturbation
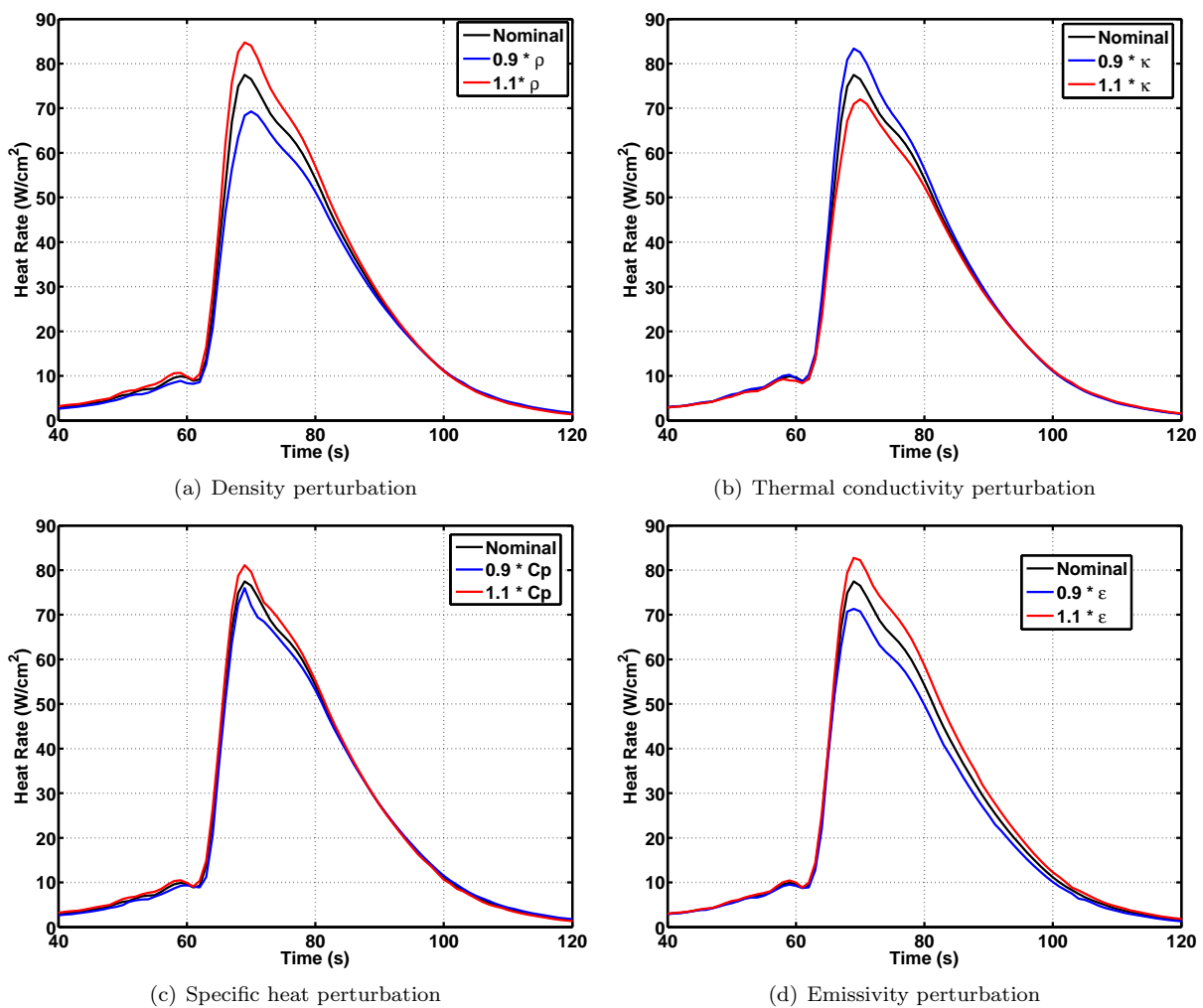
(d) Emissivity perturbation

Figure 11. Effect of material property perturbations on heating estimation results at plug 2.

that a higher thermal conductivity leads to higher heat conduction into the material, resulting in a lower surface heating required to maintain the same temperature response. Figure 11c shows the effect of specific heat perturbation. Similar to density, higher specific heat leads to a higher thermal mass which results in a higher estimated surface heating. However, the sensitivity to specific heat is far less than sensitivity to density. Finally, Fig. 11d shows the effect of surface emissivity perturbation. Higher surface emissivity leads

American Institute of Aeronautics and Astronautics

to higher reradiation and lower heat conduction into the material. Consequently, higher incoming heating is required to maintain the same in-depth response. It can also be observed that the estimation sensitivity to emissivity is significant only during the peak and post-peak regions when significant reradiation is expected due to higher wall temperature.

5. Uncertainty Quantification

A Monte Carlo analysis is performed on the inverse estimation procedure to quantify the uncertainty associated with the estimated surface heating profiles at plugs 1, 2 and 5. These plugs represent cases of low, high and medium heating levels. Each Monte Carlo iteration performs a surface heating estimation for a set of input parameters. Eight input parameters are varied in the simulation using Gaussian distributions. Table 1 provides the standard deviation for these parameters. These values are derived based on engineering judgment and material property characterization experiments conducted on material samples from the same PICA billets that the MISP flight plugs originated from. For example, the virgin density of the flight MISP plugs is measured to be within $\pm 1.5\%$ of the nominal PICA density. Assuming that this interval represents $\pm 2\sigma$ bounds, the standard deviation is estimated to be 0.75% of the nominal value. The standard deviations for other parameters are estimated in a similar manner. Char density is correlated to virgin density by using a fixed char yield value (with a 1% standard deviation) to derive the char density from virgin density. Virgin and char thermal conductivity are also correlated.

Table 1. Standard deviation for Monte Carlo simulation parameters

Parameter	Std. Dev. (% of nominal)	Parameter	Std. Dev. (% of nominal)
ρ_v	0.75%	Char yield	1% (corr.)
Cp_v	4%	Cp_c	1%
κ_v	7.5%	κ_c	10% (corr.)
$\epsilon_{v,c}$	1.5%	TC1 depth error	0.0015 inch

The Monte Carlo analysis is conducted for 2000 iterations. Then, the standard deviations are calculated as functions of time for the estimated surface heat rate profiles obtained from the Monte Carlo results. After about 1000 iterations, the peak heat rate standard deviation stabilized and did not change significantly, affirming the analysis convergence. Figures 12a-12c show the 95% confidence intervals ($\pm 1.96\sigma$) for the estimated heat rate profiles at plugs 1, 2 and 5. Figure 12d presents the estimated heat rate standard deviation as a function of time for all these three plugs.

The maximum heat rate standard deviation for plug 2 happens around the peak heating time and is about $7 \ W/cm^2$ which is almost 10% of the nominal surface heating value. The peak heat rate standard deviation for plug 1 is about $2 \ W/cm^2$ which is less than 6% of its peak heating value. It should be noted that this Monte Carlo analysis does not include the effect of recession uncertainty because the recession sensitivity is determined based on post-estimation computations and relies on an arbitrarily predefined recession profile. The recession sensitivity analysis perfomed earlier in the paper provides an indication of the expected level of uncertainty due to recession.

IV.   Material Property Estimation

Simultaneous estimation of material properties and surface heating is a challenging problem because the surface energy balance and the in-depth material response problems are tightly coupled. Therefore in this study, we use a thermocouple (TC) driver approach to estimate PICA material properties from MISP flight data. The TC driver approach has traditionally been used with arcjet data in cases where the surface boundary conditions were not characterized well. In this approach, the data from the thermocouple closest to the surface (TC1) is used as the temperature boundary condition at that thermocouple location and the in-depth heat transfer and pyrolysis problem is solved for the material stack beneath that thermocouple. This approach effectively decouples the in-depth heat transfer and surface heating problems, thus allowing the application of inverse methods to estimate material properties without the knowledge of surface heating conditions. Inverse methods estimate material properties by matching the deeper thermocouple data (TC2-4) and their corresponding FIAT predictions.
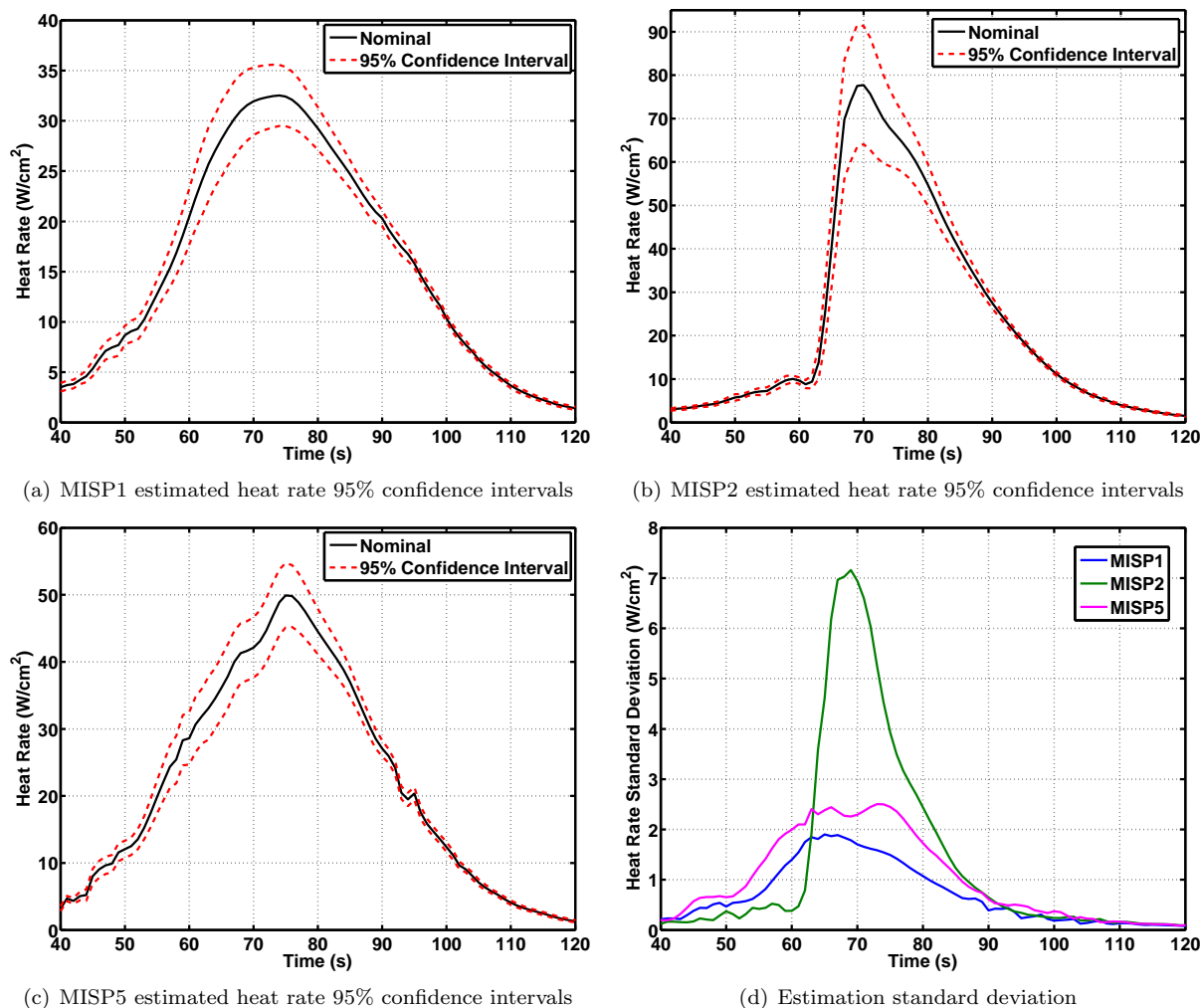
(a) MISP1 estimated heat rate 95% confidence intervals

(b) MISP2 estimated heat rate 95% confidence intervals

(c) MISP5 estimated heat rate 95% confidence intervals

(d) Estimation standard deviation

Figure 12. Heat rate estimation uncertainty at plugs 1, 2 and 5 derived from the Monte Carlo analysis.

Unlike surface heating estimation, which is a function estimation problem, material property estimation is a parameter estimation problem which faces certain unique challenges. These problems typically involve the estimation of multiple correlated parameters which could lead to non-uniqueness issues. PICA material response is characterized by multiple model parameters including decomposition, thermophysical and pyrolysis parameters such as virgin and char density, specific heat, thermal conductivity, emissivity and pyrolysis gas enthalpy. Not all these parameters are simultaneously observable from the data and therefore it is impossible to estimate all of them. For complex problems where different parameters contribute to the uncertainty, a comprehensive methodology is required to yield an accurate multi-parameter estimation. The results of an inverse estimation depend strongly on the range of measurements used in the analysis and input parameters being estimated. It is crucial that the measurement and parameter selections are performed intelligently prior to the inverse estimation. The authors previously developed a multi-parameter estimation methodology with the goal of identifying model parameters and measurement ranges that should be used in these inverse problems.[32] This methodology proposes guidelines on how to conduct the parameter estimation via four steps: nominal analysis, uncertainty analysis, sensitivity analysis, and inverse analysis.

The first three steps provide the prerequisite information to set up a successful inverse estimation. Nominal analysis examines the quality of the data and provides a direct comparison between the flight data and the model predictions (FIAT temperature predictions). The ranges of measurements that are reliable for inverse analysis is identified. Uncertainty analysis narrows down the list of material parameters to a subset representing the top contributors to the overall uncertainty. Sensitivity analysis investigates potential linear dependencies among the parameters which could cause them not to be simultaneously observable from the data. These steps provide a list of parameters to be estimated and the ranges of data that must be used in

American Institute of Aeronautics and Astronautics

the estimation process. In the last step, inverse methods are used to estimate the selected parameters from the data. This paper focuses on the material property estimation results at plug 2. Similar analyses can be performed for other plugs.

A.   Nominal Analysis

In the TC driver approach the temperature data from the shallowest thermocouple (TC1) is used as the true boundary condition and the thermal response for the underlying material is calculated using FIAT and nominal PICA properties. It should be noted that while TC1 data can be deemed as the true material temperature at TC1 depth, there is a ±0.003 inch uncertainty in the location of thermocouples. In this analysis two bounding scenarios are considered in addition to the nominal TC depths to account for their location uncertainty. In one scenario, TC1 depth is offset by +0.003 inch while TC2-4 depths are offset by −0.003 inch. This will lead to the farthest possible separation between the driver thermocouple and the underlying ones, thus resulting in a lower bound for temperature predictions. In another scenario, TC1 depth is offset by −0.003 inch while TC2-4 depths are offset by +0.003 inch leading to the closest distance between TC1 and TC2-4 and thus a higher bound for temperature predictions. In this paper, results from these scenarios are respectively labeled as "lower" and "upper" bounds.
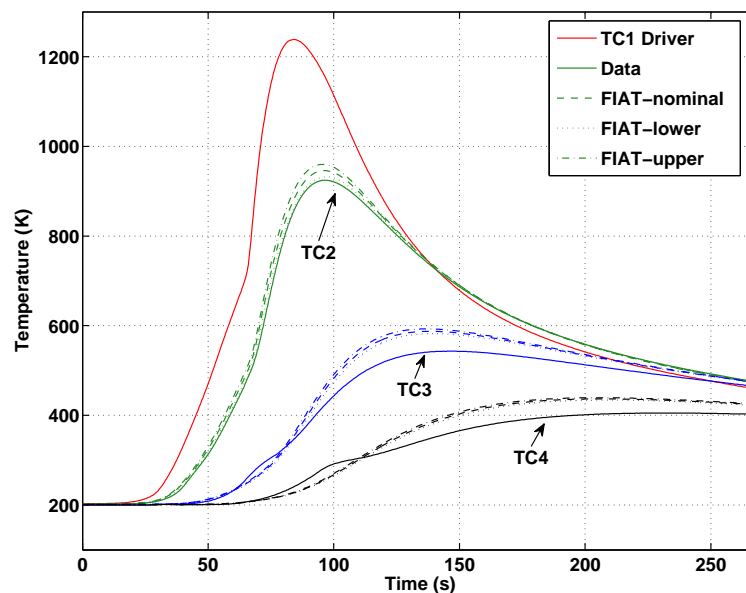

Figure 13. FIAT predictions compared to flight temperature data using a TC1 driver approach at plug 2.

Figure 13 shows the comparison between the FIAT predictions and TC2-4 flight temperature data using a TC1 driver approach at plug 2. The lower and upper-bound FIAT predictions are presented in addition to the nominal predictions. It can be observed that the nominal FIAT solutions slightly overpredict the flight data at TC2 location; however, the flight temperatures are very close to the lower bound of the FIAT temperature predictions. At TC3-4 locations, all three FIAT solutions significantly overpredict the flight data. Considering the fact that TC3-4 are mainly in the virgin material, this overprediction is indicative of inaccuracies in virgin material properties. We can also see that there is an unexpected slope change ("hump") in the TC3-4 temperature profiles. The hump happens in the 200-400 K temperature range. This trend is observed consistently for all plug locations. Similar behavior has also been seen in the MISP qualification arcjet dataset, in arcjet testing for some materials other than PICA, and also for Mars Pathfinder bondline thermocouple data. This phenomenon is not well understood at present, but is believed to be associated with some type of material or instrument-related process. Current analysis tools are not able to model this behavior; therefore, we should not expect a match between the data and model predictions for this part of the data. For this reason, the TC3-4 data range used here in inverse analysis is limited to the time after the clearance of the slope change. This corresponds to the time period after about 92 and 195 seconds for TC3 and TC4 respectively.

American Institute of Aeronautics and Astronautics

B.   Uncertainty and Sensitivity Analysis

The goal of uncertainty analysis is to define the material properties that contribute the most to the uncertainty in the heatshield material in-depth thermal response. The approach employed to accomplish this goal is probabilistic, and is accomplished with Monte Carlo simulations. We start with a complete list of material parameters and down-select to a smaller subset containing parameters of most importance that should be estimated by inverse methods. This analysis should not be confused with the Monte Carlo analysis presented in the previous section which was performed around the inverse analysis procedure to determine uncertainties in the estimated surface heating. Unlike that analysis, this Monte Carlo simulation is performed around the forward analysis by varying material properties and recording the material in-depth temperature response. The input probability distributions shown in Table 1 for material properties are also used here with the addition of pyrolysis gas enthalpy, h_g. A Gaussian distribution with a standard deviation of 7.5% of the nominal value is applied for this parameter.[33] To ensure statistical accuracy, 10,000 runs are performed. Upon the completion of the Monte Carlo simulations, a linear regression analysis of the results is performed to calculate the uncertainty contribution of the material properties to in-depth temperature response. Figure 14 shows the uncertainty contribution of different properties to TC2 and TC3 temperature as a function of time. The results for TC4 are not shown here because they are very similar to TC3 results. We can clearly see that the virgin and char thermal conductivity are the top contributors to both TC2 and TC3 temperature uncertainty followed by the virgin and char specific heat.

(a) Temperature uncertainty contribution at TC2   (b) Temperature uncertainty contribution at TC3
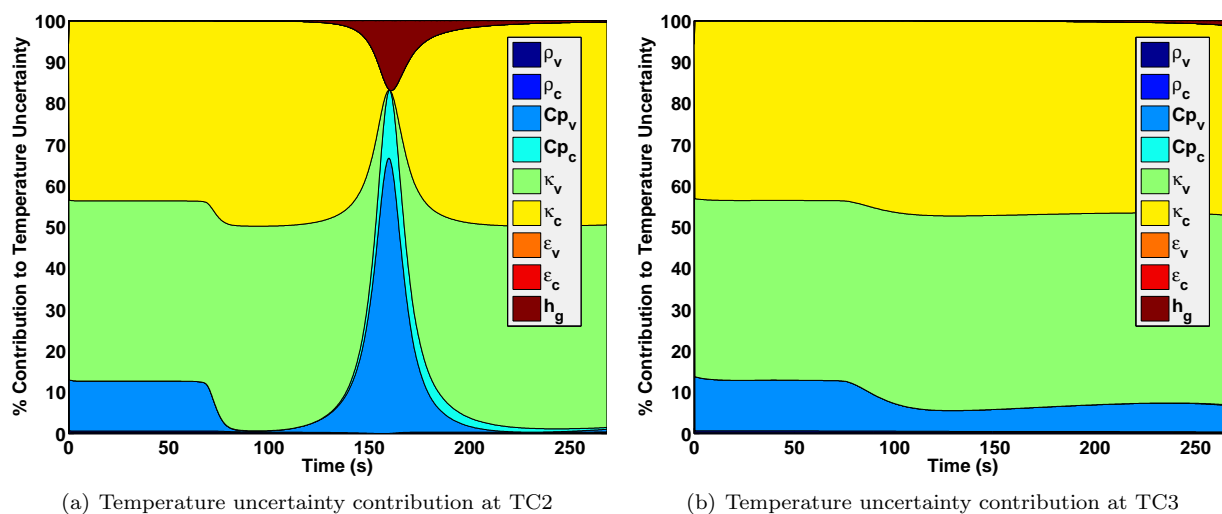
Figure 14.   Material property contribution to in-depth temperature uncertainty at plug 2.

Before any attempt to estimate these parameters, a sensitivity analysis must be performed to examine the level of linear dependency among them. In inverse parameter estimation problems, it is challenging to estimate highly dependent input parameters simultaneously because that leads to non-unique solutions and inaccurate estimates of the parameters. Therefore, in such multi-parameter estimation problems it is imperative to conduct a sensitivity analysis beforehand. In this analysis, each parameter is perturbed independently by a small amount ($\pm 0.5\%$) and the change in in-depth temperature is recorded. Figure 15 shows the results of this sensitivity analysis for TC2 and TC3 locations at plug 2. Only the parameters that have been identified as the top uncertainty contributors are included in this step. Examination of the shape and magnitude of these plots gives an indication of the level of correlation between these parameters. There is a strong correlation between specific heat and thermal conductivity. The reason for this behavior is that the heat transfer through the material is mainly driven by thermal diffusivity which is directly proportional to the thermal conductivity and inversely proportional to the specific heat. Therefore increasing one or reducing the other one will have the same effect on the in-depth temperature response. These strong correlations mean that in the presence of measurement errors these parameters cannot be estimated simultaneously as they are not independently observable from the flight temperature data.
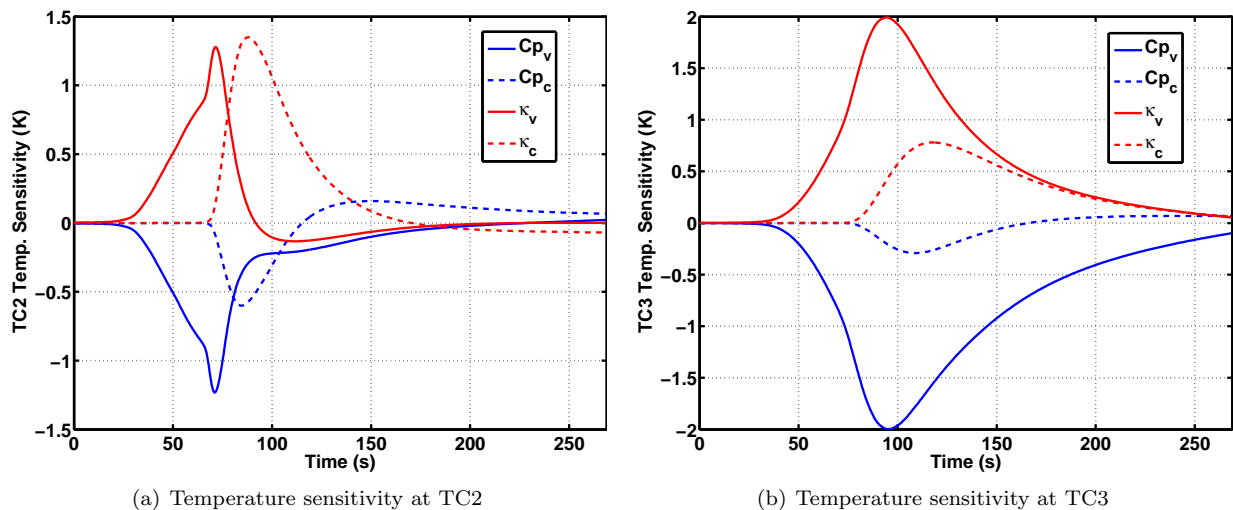
American Institute of Aeronautics and Astronautics

(a) Temperature sensitivity at TC2   (b) Temperature sensitivity at TC3

Figure 15. Plug 2 in-depth temperature sensitivity to one-by-one perturbations in material properties.

C. Inverse Analysis

Uncertainty and sensitivity analyses helped us determine that virgin and char thermal conductivity are not linearly dependent and contribute the most to in-depth temperature uncertainty. Through nominal analysis, we also identified the range of TC2-4 measurements that should be used in the inverse analysis. Now, we apply inverse parameter estimation methods to the TC driver problem to estimate these two parameters by matching FIAT temperature predictions and TC2-4 flight data. Similar to heating reconstruction, the estimation is done by minimizing an objective function comprised of the sum of squared differences between FIAT predictions and flight data. The minimization is performed using the Levenberg-Marquardt method. This method is commonly used in literature for parameter estimation problems. It was originally derived by Levenberg[34] and later modified by Marquardt.[35] This technique was derived as an iterative method that would tend to the Gauss-Newton method in the neighborhood of the minimum and would tend to the steepest descent method in the neighborhood of the initial guess. This is done using a damping parameter which reduces oscillations and instabilities due to the ill-conditioned nature of inverse heat transfer problems in the region around the initial guess. The detailed algorithm for this method can be found in reference 32.

The inverse analysis is performed for the lower and upper bound scenarios in addition to the nominal TC depths. This will allow us to capture the expected range of the parameter estimates due to the TC depth uncertainty. Table 2 shows the estimates for PICA virgin and char conductivity at plug 2. The estimates given here are scaling factors multiplied by the entire temperature-dependent thermal conductivity curve. For example, a value of 0.9 would mean a 10% reduction in the thermal conductivity nominal value at all temperatures.

Table 2. Material property estimation results for plug 2

Parameter	Estimate	Lower-Bound Estimate	Upper-Bound Estimate
Virgin Conductivity	0.7902	0.8079	0.7749
Char Conductivity	0.7878	0.8714	0.7051

The inverse estimation requires about 20% reduction in both virgin and char thermal conductivity to provide a better match the flight data. We can see that the sensitivity of char conductivity estimate to TC depth uncertainty is much greater than virgin conductivity. Figure 16 shows the comparison of TC2-4 flight temperature data with the nominal and post-estimation FIAT predictions. These plots are generated for the nominal TC depth scenario. We can clearly see that a better match between FIAT predictions and flight data is achieved after inverse estimation of virgin and char thermal conductivity. The root mean square of errors is reduced by a factor of almost four.

It should be noted that the material property estimation analysis presented here can easily be extended to other plugs and other thermocouple driver possibilities. For example, one can conduct this analysis
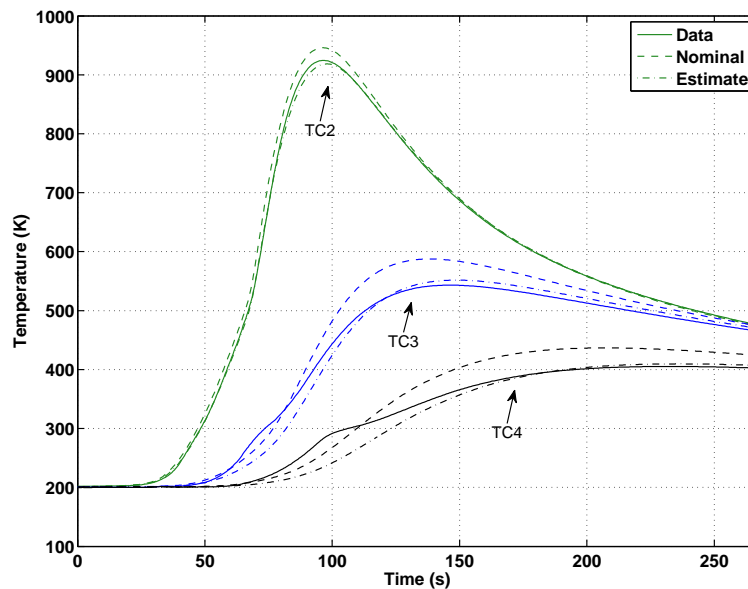
American Institute of Aeronautics and Astronautics

Figure 16. Flight temperature data compared with the nominal and post-estimation FIAT prediction for plug 2 TC1 driver.

for a TC2 or TC3 driver at plug 1 to focus mainly on virgin properties. In each one of these cases, a separate uncertainty and sensitivity analysis can be performed to identify the properties that should be estimated. Unfortunately, all these possibilities currently can not be explored due to the observed slope change ("hump") in the TC3-4 data which significantly reduces the confidence in the inverse estimates. Further material property estimation work should be pursued once this behavior is understood and modeled in the analytical tools. Furthermore, the current analysis estimated the virgin and char conductivity by uniformly scaling their temperature-dependent curve. In future, temperature-dependent estimation of these properties can also be pursued to obtain more accurate conductivity curves.

V. Conclusions

An inverse analysis of the MSL entry vehicle aeroheating environment and thermal protection system response was performed in this paper based on heatshield flight temperature data. The time-dependent surface heating at MISP plug locations was reconstructed from the shallowest thermocouple flight data using two different approaches. The first approach estimated the heat transfer coefficient profile while relying on PICA equilibrium chemistry models to calculate surface ablation terms. A disadvantage of this approach is the fact that equilibrium chemistry models are known to overpredict surface recession at MSL heating conditions. Consequently, another bounding approach was considered where the surface heating was directly estimated assuming a non-receding material surface. This work also investigated the effect of numerical parameters, measurement errors, recession uncertainty, and material property perturbations on the estimated surface heating profiles. Finally, a Monte Carlo analysis was performed for three plug locations to determine the uncertainty bounds associated with the estimated surface heating.

Additionally, certain material properties were inversely estimated using a TC driver approach. In this approach, the data from the shallowest thermocouple were used for the true boundary condition and material properties were estimated to match FIAT predictions with the underlying thermocouple flight data. A four-step methodology was utilized to determine which material properties should be estimated and what range of temperature data should be used in the estimation. A Monte Carlo analysis was performed to determine the most important material properties based on their contribution to in-depth temperature uncertainty. A sensitivity analysis was conducted to investigate the level of linear dependency among the material properties to determine which parameters are simultaneously observable from the data. Finally, virgin and char thermal conductivity were estimated by using inverse methods to match FIAT predictions with flight data. This analysis was performed for plug 2 only but can easily be extended to other plugs.

American Institute of Aeronautics and Astronautics

The estimated heating profiles for the leeside plugs (2, 3, and 6) match the CFD predictions although the turbulent heating augmentation is slightly lower than predictions. Plugs 5 and 7, which are located around the apex region, experienced significantly higher heating than CFD predictions. The proximity of these plugs to the location of turbulent transition and possible shock-layer radiative heating could explain this phenomenon, although a more detailed investigation is required. The estimated heat rate profile at the stagnation region plugs (1 and 4) are slightly higher than CFD predictions which can be explained partially by radiative heating. A more detailed radiative heating analysis is suggested for future work. The estimated surface heating profiles were shown to be sensitive to surface recession. A more accurate PICA recession model for MSL heating conditions can significantly reduce estimation uncertainties.

The TC driver approach showed that the nominal PICA model overpredicts the temperature profile at TC3 and TC4 location consistently for all the plugs which is indicative of inaccuracy of virgin properties. Furthermore, a slope change was observed in the 200-400 K range in the temperature profiles of TC3 and TC4. This behavior has been seen in other ground and flight datasets. Further analysis is needed to understand the source of this behavior and develop relavent modeling capabilities.

Acknowledgments

References

[1]Wright, M., Chun, T., Edquist, K., Hollis, B., Krasa, P., and Campbell, C., "A Review of Aerothermal Modeling for Mars Entry Missions," *48th AIAA Aerospace Sciences Meeting*, AIAA 2010-44, January 2010.

[2]Ingoldby, R., Michel, F., Flaherty, T., Doryand, M., Preston, B., Villyard, K., and Steele, R., "Entry Data Analysis for Viking Landers 1 and 2 Final Report," NASA CR-159388, Martin Marietta Corporation, 1976.

[3]Schmitt, D., "Base Heating on a an Aerobraking Oribital Transfer Vehicle," *21st AIAA Aerospace Sciences Meeting*, AIAA 83-0408, Reno, Nevada, January 1983.

[4]Edquist, K., Wright, M., and Allen, G., "Viking Afterbody Heating Computations and Comparisons to Flight Data," *44th AIAA Aerospace Sciences Meeting*, AIAA 2006-386, Reno, Nevada, January 2006.

[5]Milos, F., Chen, Y., Congdon, W., and Thornton, J., "Mars Pathfinder Entry Temperature Data, Aerothermal Heating, and Heatshield Material Response," *Journal of Spacecraft and Rockets*, Vol. 36, No. 3, 1999, pp. 380–391.

[6]Mahzari, M., White, T., and Braun, R., "Reconstruction of Mars Pathfinder Aeroheating and Heat Shield Response Using Inverse Methods," *Journal of Spacecraft and Rockets*, 2013.

[7]Steltzner, A., Kipp, D., Chen, A., Burkhart, P., Guernsey, C., Mendeck, G., Mitcheltree, R., Powell, R., Rivellini, T., Martin, A. S., and Way, D., "Mars Science Laboratory entry, descent and landing system," *IEEE Aerospace Conference*, IEEEAC1497, Big Sky, MT, March 2006.

[8]Tran, H., Johnson, C., Rasky, D., Hui, F., Chen, Y., and Hsu, M., "Phenolic Impregnated Carbon Ablators (PICA) for Discovery Class Mission," *31st AIAA Thermophysics Conference*, AIAA 1996-1911, New Orleans, LA, June 1996.

[9]Edquist, K., Dyakonov, A., Wright, M., and Tang, C., "Aerothermodynamic Design of the Mars Science Laboratory Heatshield," *41st AIAA Thermophysics Conference*, AIAA 2009-4075, San Antonio, Texas, June 2009.

[10]Beck, R., Driver, D., Wright, M., Laub, B., Hwang, H., Slimko, E., Edquist, K., Sepka, S., Willcockson, W., and Thames, T., "Development of the Mars Science Laboratory Heatshield Thermal Protection System," *41st AIAA Thermophysics Conference*, AIAA 2009-4229, San Antonio, Texas, June 2009.

[11]Wright, M., Beck, R., Edquist, K., Driver, D., Sepka, S., Slimko, E., Willcockson, W., DeCaro, A., and Hwang, H., "Sizing and Margins Assessment of the Mars Science Laboratory Aeroshell Thermal Protection System," *41st AIAA Thermophysics Conference*, AIAA 2009-4231, San Antonio, Texas, June 2009.

[12]Gazarik, M., Wright, M., Little, A., Cheatwood, F., Herath, J., Munk, M., Novak, F., and Martinez, E., "Overview of the MEDLI Project," *IEEE Aerospace Conference*, IEEE 2008-1510, Big Sky, Montana, March 2008.

[13]Mahzari, M., Braun, R., White, T., and Bose, D., "Preliminary Analysis of the Mars Science Laboratory's Entry Aerothermodynamic Environment and Thermal Protection System Performance," *51st AIAA Aerospace Sciences Meeting*, AIAA 2013-0185, Grapevine, Texas, January 2013.

[14]Bose, D., White, T., Santos, J., Feldman, J., Mahzari, M., Olson, M., and Laub, B., "Initial Assessment of Mars Science Laboratory Heat Shield Instrumentation and Flight Data," *51st AIAA Aerospace Sciences Meeting*, Dallas, Texas, 2013.

[15]Bose, D., White, T., Mahzari, M., and Edquist, K., "A Reconstruction of Aerothermal Environment and Thermal Protection System Response of the Mars Science Laboratory Entry Vehicle," *23rd AAS/AIAA Spaceflight Mechanics Meeting*, AAS 13-311, Kauai, Hawaii, February 2013.

[16]Bose, D., Santos, J., Rodriguez, E., White, T., and Mahzari, M., "Mars Science Laboratory Heat Shield Instrumentation and Arc Jet Characterization," *44th AIAA Thermophysics Conference*, AIAA 2013-2778, San Diego, CA, June 2013.

American Institute of Aeronautics and Astronautics

[17]White, T., Mahzari, M., Bose, D., and Santos, J., "Post-fight Analysis of Mars Science Laboratory's Entry Aerothermal Environment and Thermal Protection System Response," *44th AIAA Thermophysics Conference*, AIAA 2013-2779, San Diego, CA, June 2013.

[18]Edquist, K., Hollis, B., Johnston, C., Bose, D., White, T., and Mahzari, M., "Mars Science Laboratory Heatshield Aerothermodynamics: Design and Reconstruction," *44th AIAA Thermophysics Conference*, AIAA 2013-2781, San Diego, CA, June 2013.

[19]White, T., Cozmuta, I., Santos, J., Laub, B., and Mahzari, M., "Proposed Analysis Process for Mars Science Laboratory Heat Shield Sensor Plug Flight Data," *42nd AIAA Thermophysics Conference*, AIAA 2011-3957, Honolulu, Hawaii, June 2011.

[20]Oishi, T., Martinez, E., and Santos, J., "Development and Application of a TPS Ablation Sensor for Flight," *46th AIAA Aerospace Sciences Meeting*, AIAA 2008-1219, January 2008.

[21]Santos, J., Jacobs, T., and Martinez, E., "Isotherm Sensor Calibration Program for Mars Science Laboratory Heat Shield Flight Data Analysis," *42nd AIAA Thermophysics Conference*, AIAA 2011-3955, Honolulu, Hawaii, June 2011.

[22]Milos, F., "Galileo Probe Heat Shield Ablation Experiment," *31st AIAA Thermophysics Conference*, AIAA 1996-1823, New Orleans, LA, June 1996.

[23]Cheatwood, F. and Gnoffo, P., "Users Manual for the Langley Aerothermal Upwind Relaxation Algorithm (LAURA)," NASA TM-4674, April 1996.

[24]Wright, M., White, T., and Mangini, N., "Data Parallel Line Relaxation (DPLR) Code User Manual; Acadia-Version 4.01.1," NASA TM 2009-215388, Oct. 2009.

[25]Chen, Y. and Milos, F., "Ablation and Thermal Response Program for Spacecraft Heatshield Analysis," *Journal of Spacecraft and Rockets*, Vol. 36, No. 3, 1999, pp. 475–483.

[26]Ozisik, M. and Orlande, H., *Inverse Heat Transfer: Fundamentals and Applications*, Taylor and Francis, New York, 2000.

[27]Beck, J. and Arnold, K., *Parameter Estimation in Engineering and Science*, Wiley, New York, 1977.

[28]Beck, J., Blackwell, B., and Clair, C. S., *Inverse Heat Conduction, Ill-posed Problems*, Wiley, New York, 1985.

[29]Tikhonov, A. and Arsenin, V., *Solution of Ill-Posed Problems*, Winston and Sons, Washington, DC, 1977.

[30]Mahzari, M. and Braun, R., "Time-Dependent Mars Entry Aeroheating Estimation from Simulated In-Depth Heat Shield Temperature Measurements," *Journal of Thermophysics and Heat Transfer*, 2013.

[31]Milos, F., Chen, Y., and Gokcen, T., "Nonequilibrium Ablation of Phenolic Impregnated Carbon Ablator," *48th AIAA Aerospace Sciences Meeting*, AIAA 2010-981, Orlando, Florida, January 2010.

[32]Mahzari, M., Cozmuta, I., Clark, I., and Braun, R., "An Inverse Parameter Estimation Methodology for the Analysis of Aeroheating and Thermal Protection System Experimental Data," *42nd AIAA Thermophysics Conference*, AIAA 2011-4027, Honolulu, Hawaii, June 2011.

[33]Sepka, S. and Wright, M., "A Monte Carlo Approach to FIAT Uncertainties- Improvements and Applications for MSL," *41st AIAA Thermophysics Conference*, AIAA 2009-4243, June 2009.

[34]Levenberg, K., "A Method for the Solution of Certain Non-linear Problems in Least Squares," *Quart. Appl. Math.*, Vol. 2, 1944, pp. 164–168.

[35]Marquardt, D., "An Algorithm for Least-Squares Estimation of Nonlinear Parameters," *Journal of the Society for Industrial and Applied Mathematics*, Vol. 11, No. 2, 1963, pp. 431–441.

American Institute of Aeronautics and Astronautics